

University of Mississippi

eGrove

Faculty and Student Publications

Physics and Astronomy

2-1-2022

Corrected Tilt Calculation for Atmospheric Pressure-Induced Seismic Noise

Richard Raspet
University of Mississippi

Craig J. Hickey
University of Mississippi

Bipin Koirala
Georgia Institute of Technology

Follow this and additional works at: https://egrove.olemiss.edu/physics_facpubs



Part of the [Astrophysics and Astronomy Commons](#)

Recommended Citation

Raspet, R., Hickey, C. J., & Koirala, B. (2022). Corrected tilt calculation for atmospheric pressure-induced seismic noise. *Applied Sciences*, 12(3), 1247. <https://doi.org/10.3390/app12031247>

This Article is brought to you for free and open access by the Physics and Astronomy at eGrove. It has been accepted for inclusion in Faculty and Student Publications by an authorized administrator of eGrove. For more information, please contact egrove@olemiss.edu.

Article

Corrected Tilt Calculation for Atmospheric Pressure-Induced Seismic Noise

Richard Raspet ¹, Craig J. Hickey ^{1,*} and Bipin Koirala ²

¹ National Center for Physical Acoustics, University of Mississippi, University, MS 38677, USA; raspet@olemiss.edu

² Guggenheim School of Aerospace Engineering, Georgia Institute of Technology, Atlanta, GA 30332, USA; bkoirala3@gatech.edu

* Correspondence: chickey@olemiss.edu; Tel.: +1-662-915-5963

Featured Application: This paper demonstrates that the behavior of the horizontal component of seismic wind noise with depth is much more complex than previously published. This fact will motivate increased use of the horizontal component in seismic wind noise studies and should lead to better determination of ground properties using inversion of measured seismic wind noise.

Abstract: In a literature search on the coupling of wind-generated pressure fluctuations into seismic noise, it was noticed that the expression for the angular tilt induced by pressure fluctuations in the seminal paper “*A preliminary investigation into the relationship between long-period seismic noise and local fluctuations in the atmospheric pressure*” by G. G. Sorrells was only valid at the surface. A search of the literature which cites the Sorrells paper was performed to see if any subsequent research corrected this error, and what effect the error might have on the research. A recent paper by Tanimoto and Wang notes the correct expression for the tilt, but employs the simpler erroneous expression in the research. In this paper, we develop the correct expression for effective measured displacements and approximate expressions analogous to those of Sorrells. The resulting magnitudes and decay with depth are then displayed and compared to Sorrells. Next, the results of the literature search are discussed. The results of three papers are identified as potentially modified by the correction of the tilt calculation. Finally, it is noted that the majority of the papers referenced are not affected by the correction, since many of the papers are for near-surface displacements of very low frequencies.

Keywords: tilt; wind-noise; seismic; horizontal component



Citation: Raspet, R.; Hickey, C.J.; Koirala, B. Corrected Tilt Calculation for Atmospheric Pressure-Induced Seismic Noise. *Appl. Sci.* **2022**, *12*, 1247. <https://doi.org/10.3390/app12031247>

Academic Editor: Andrea Paglietti

Received: 10 September 2021

Accepted: 20 January 2022

Published: 25 January 2022

Publisher’s Note: MDPI stays neutral with regard to jurisdictional claims in published maps and institutional affiliations.



Copyright: © 2022 by the authors. Licensee MDPI, Basel, Switzerland. This article is an open access article distributed under the terms and conditions of the Creative Commons Attribution (CC BY) license (<https://creativecommons.org/licenses/by/4.0/>).

1. Introduction

In the process of reviewing the literature of wind-generated pressure fluctuation coupling into the ground as part of a research effort [1,2], the paper “*A preliminary investigation into the relationship between long-period seismic noise and local fluctuations in the atmospheric pressure field*” by Gordon G. Sorrells [3] was studied. It was noted that Sorrells’s expression for the ground tilt due to passage of a pressure wave was not complete for sensors below the surface. A complete review of peer-reviewed literature which referenced Sorrells revealed that Tanimoto and Wang [4] had identified the correct expression but had not used it in their research. In this paper, we use the complete expression to analyze apparent subsurface ground motion due to plane wave propagating harmonic pressure fluctuations caused by the wind, and highlight the frequency and depth regimes where the complete expression must be used.

Section 2 first reviews the theory of coupling of slow-moving plane wave pressure fluctuations into vertical and horizontal ground displacements, as presented by Sorrells [3]. Then, expressions for the correction of apparent horizontal displacement due to the complete term of the tilting of the sensor in the medium are derived and compared to Sorrells’s

expression. For discussion purposes, the analytic approximations corresponding to Sorrells’s approximation are derived.

Section 3 presents numerical calculations of the corrected total measured displacements at the surface for Sorrells’s models 1, 2b, and 4 of the ground, and the attenuation with depth for Sorrells’s Model 4. The results for the measured horizontal displacement display significant changes from calculations using with the incomplete tilt expressions.

Section 4 reviews the impact of the use of the correct complete expression for the tilt on the literature which reference Sorrells’s [3] paper. Many of the papers are unaffected since they study near-surface displacements or investigate very low-frequency excitations. A few papers for which the correction may affect the results are examined in detail.

Section 5 summarizes the findings of the research and discusses possible research which is motivated by the more complex dependence of the horizontal displacement with depth of the complete expression for tilt.

2. Theory

2.1. Displacement

The theory of coupling of plane pressure waves into a homogenous elastic half-space is summarized in this section as background for the research presented herein. The basic setup follows Sorrells [3] in the notation of Brekhovskikh [5].

Consider the two-dimensional problem where x and z are the Cartesian coordinates in directions parallel and normal to the surface of the ground, as shown in Figure 1. The normal component z denotes the depth into the ground. The wind moving at a speed c in the x -direction creates pressure fluctuations in local space defined by:

$$P(x, t) = P_0 e^{i(kx - \omega t)} \tag{1}$$

where P_0 is the amplitude of the local pressure. The angular frequency is ω and the horizontal component of wave number, k , is given by

$$k = \frac{\omega}{c} \tag{2}$$

where c is the speed of the wind, and is much less than the acoustic velocity and the seismic velocity.

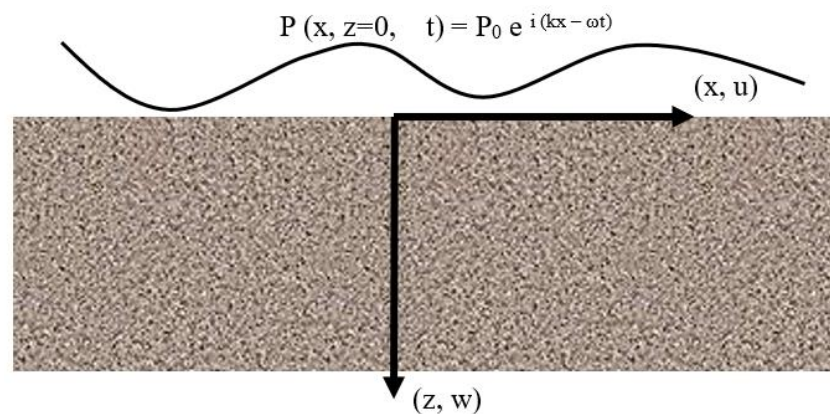


Figure 1. Coordinate systems and displacements (u, w) of an elastic half-space.

In general, a displacement vector can be expressed in terms of a scalar potential, φ , and a vector potential, ψ , as

$$\vec{a} = \nabla\varphi + \nabla \times \vec{\psi}. \tag{3}$$

These potentials obey the following wave equations:

$$\nabla^2\varphi = \frac{1}{\alpha^2} \frac{\partial^2\varphi}{\partial t^2} \tag{4}$$

and

$$\nabla^2 \psi = \frac{1}{\beta^2} \frac{\partial^2 \psi}{\partial t^2} \tag{5}$$

where α and β are compressional and shear wave speed, respectively. For an isotropic elastic solid, the waves' speeds are related to Lamé's elastic constants (λ and μ) and mass density (ρ) as

$$\alpha^2 = \frac{\lambda + 2\mu}{\rho} \tag{6}$$

and

$$\beta^2 = \frac{\mu}{\rho}. \tag{7}$$

For the problem considered here, the wind-induced seismic vibrations will decay with an increase in depth and frequency, such that the scalar potential for the compressional wave is

$$\varphi = \varphi_0 e^{-\gamma z} e^{i(kx - \omega t)} \tag{8}$$

and the vector potential for the shear wave is

$$\psi = \psi_0 e^{-\delta z} e^{i(kx - \omega t)}. \tag{9}$$

Here, δ and γ give the attenuation in the z-direction for the shear and compression wave, respectively:

$$\delta = \sqrt{k^2 - \left(\frac{\omega}{\beta}\right)^2} \tag{10}$$

$$\gamma = \sqrt{k^2 - \left(\frac{\omega}{\alpha}\right)^2}. \tag{11}$$

Since the pressure disturbance given in Equation (1) is of the form $e^{i(kx - \omega t)}$, then $\frac{\partial}{\partial x} = ik$ and $\frac{\partial}{\partial t} = -i\omega$. The horizontal displacement (u) is related to the potentials as

$$u = ik\varphi - \frac{\partial \psi}{\partial z} \tag{12a}$$

or

$$u = i(\varphi_0 k e^{-\gamma z} + \psi_0 \delta e^{-\delta z}) e^{i(kx - \omega t)} \tag{12b}$$

and the vertical displacement (w) as

$$w = \frac{\partial \varphi}{\partial z} + ik\psi \tag{13a}$$

or

$$w = \left(-\varphi_0 \gamma e^{-\gamma z} + i\psi_0 k e^{-\delta z}\right) e^{i(kx - \omega t)}. \tag{13b}$$

The ground motion is induced by the wind pressure (stress) across the ground surface. Therefore, this problem is formulated as a boundary value problem with appropriate boundary conditions. The usual boundary conditions are that the components of the displacement vector should be continuous, and the components of the stress tensor (or tractions, Z_i) should be continuous at the boundary. The three traction components for the two-dimensional problem considered here are

$$Z_z = \lambda \left(\frac{\partial u}{\partial x} + \frac{\partial w}{\partial z} \right) + 2\mu \left(\frac{\partial w}{\partial z} \right) \tag{14a}$$

$$Z_x = \mu \left(\frac{\partial u}{\partial z} + \frac{\partial w}{\partial x} \right) \tag{14b}$$

$$Z_y = 0 \tag{14c}$$

The boundary conditions at the ground surface ($z = 0$) are given by

$$Z_z = \lambda \left(\frac{\partial u}{\partial x} + \frac{\partial w}{\partial z} \right) + 2\mu \left(\frac{\partial w}{\partial z} \right) = -P_o e^{i(kx - \omega t)} \Big|_{z=0} \tag{15a}$$

and

$$Z_x = \mu \left(\frac{\partial u}{\partial z} + \frac{\partial w}{\partial x} \right) = 0 \Big|_{z=0}. \tag{15b}$$

Solving Equation (15) for specified ground properties (λ , μ , or α , β , and ρ), frequency (ω), wind speed (c), and the associated pressure (P_o), we obtain values for the potentials φ_0 and ψ_0 . Substituting this solution into Equations (12b) and (13b) provides the horizontal and vertical displacement at a depth, z , below ground surface. The induced waves are in the form of Rayleigh waves.

2.2. Apparent Horizontal Displacement Due to Tilt

Tilt noise is a pseudo-signal measured by a mass-based seismic sensor when the instrument is tilted from its level position by an angle θ , thereby changing the direction of gravitational force on the seismic mass. Variations in the local atmospheric pressure are a prime cause of tilt in the ground, which results in increased horizontal seismic noise in the long-period band. This tilt noise restricts the use of horizontal data for sensitive seismological studies.

Figure 2 shows a schematic sketch of a two-component sensor (geophone), represented by masses on springs, that is affected by tilt as the ground undergoes a period of deformation. The sensor shown in the figure is experiencing a positive tilt by an angle θ with respect to the vertical, and g is the acceleration due to gravity. The horizontal (x) component experiences an increase in force, whereas the vertical (z) component experiences a reduction in force due to tilt. The horizontal displacement at a single angular frequency (ω), corresponding to the apparent acceleration, is given by

$$u_{\text{tilt}} = -\frac{g}{\omega^2} \sin \theta \approx -\frac{g}{\omega^2} \theta. \tag{16}$$

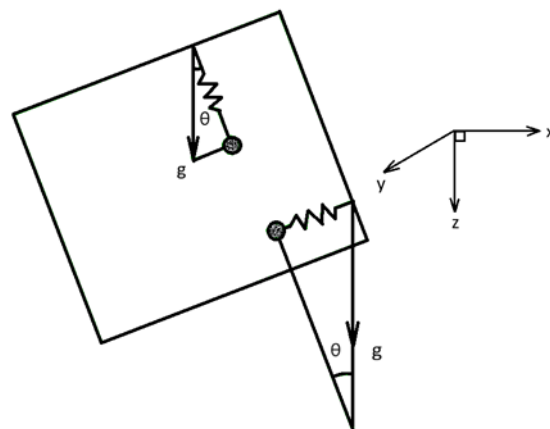


Figure 2. Mass-spring representation of a horizontal and vertical component geophone.

The negative sign indicates that the apparent displacement is negative for a positive rotation and the effect goes to zero when the tilt is zero. The vertical displacement from equilibrium, w , at a single angular frequency (ω), corresponding to the apparent acceleration, is given by

$$w_{\text{tilt}} = -\frac{g}{\omega^2} (1 - \cos \theta). \tag{17}$$

The negative sign indicates that the tilt effect is an upward displacement (reduced elongation of the spring) due to reduced force acting along the direction of the spring. The effect of tilt on the vertical component, w , is second-order.

The expression for the tilt angle, θ , appropriate to a sensor on the surface is

$$\tan \theta = -\frac{\Delta w}{\Delta x} \approx -\frac{\partial w}{\partial x} \approx \theta \tag{18}$$

for small θ . We note that Sorrells [3] has a similar equation with the opposite sign. Since he only discusses magnitude and does not combine the tilt contribution with the actual horizontal displacement, this introduces no error. We present Sorrells’s result converted to our sign convention below.

Since we are interested in investigating the combined response over a wide range of frequencies and as a function of depth, we calculate the effective horizontal displacement as

$$u_{\text{effective}} = u + u_{\text{tilt}} \tag{19}$$

where u is the actual displacement, u_{tilt} is the effect of tilt, and $u_{\text{effective}}$ is the effective displacement measured by a mass-based sensor.

In elastic media, the angle of tilt inside the medium induced by displacements is given by [6]

$$\theta = \frac{1}{2} (\nabla \times \vec{u}) \tag{20}$$

which in our coordinate system is

$$\theta = \frac{1}{2} \left(\frac{\partial u}{\partial z} - \frac{\partial w}{\partial x} \right) \tag{21}$$

Combining Equations (16), (19) and (21) gives the effective horizontal displacements as

$$u_{\text{effective}} = u - \frac{g}{2\omega^2} \left(\frac{\partial u}{\partial z} - \frac{\partial w}{\partial x} \right) \tag{22}$$

Substituting in the expressions for the displacements in terms of potentials, Equations (12b) and (13b), into Equation (22), the generalized expression for the effective horizontal displacement is

$$u_{\text{effective}} = u - \frac{g}{2\omega^2} \left(\frac{\omega}{\beta} \right)^2 \psi = u - \frac{g}{2\beta^2} \psi \tag{23}$$

which is valid throughout the elastic half-space. At the ground surface, it is assumed that there is no horizontal stress, Equation (15b), imposing the condition

$$\frac{\partial u}{\partial z} = -\frac{\partial w}{\partial x} \tag{24}$$

Substituting condition Equation (24) into the second term of Equation (22) provides the expression for tilt at the surface:

$$u_{\text{tilt}} = \frac{g}{\omega^2} \frac{\partial w}{\partial x} \Big|_{z=0} \tag{25}$$

Sorrells [3] uses the surface expression for the tilt angle, Equation (18), which results in an expression equivalent to Equation (25). However, the actual tilt contribution will differ for locations within the ground.

2.3. Analytic Approximations

Sorrells presents approximate results for u , w , and u_{tilt} . Two approximations are employed. First, he notes that c , the wind speed, is much lower than the seismic speeds, so

the vertical attenuations γ and δ can be expanded to first-order. Next, Sorrells notes the following for low frequency:

$$|\omega|z \ll \frac{2\beta^2}{c} < \frac{2\alpha^2}{c} \tag{26}$$

and the exponential terms $e^{-\delta z}$ and $e^{-\gamma z}$ can be expanded about $e^{-\frac{\omega z}{c}}$. The exact term, Equation (23), has been approximated to the same order. The figures in this paper are calculated exactly from the theory using MATLAB [7]. The approximate forms useful for discussing the general behavior are presented below. The signs have been adjusted to conform with our use of the $e^{-i\omega t}$ notation and stress due to pressure as $-P_o$. These terms are:

Horizontal displacement:

$$u = \frac{icP_o}{2\mu\omega} \left[\frac{\mu}{\lambda + \mu} - \frac{\omega z}{c} \right] e^{-\frac{\omega z}{c}} e^{i(kx - \omega t)} \tag{27}$$

Vertical displacement:

$$w = \frac{cP_o}{2\mu\omega} \left[\frac{\lambda + 2\mu}{\lambda + \mu} + \frac{\omega z}{c} \right] e^{-\frac{\omega z}{c}} e^{i(kx - \omega t)} \tag{28}$$

Tilt contribution:

$$u_{\text{tilt}} = \frac{ig}{\omega^2} \frac{P_o}{2\mu} \left[\frac{\lambda + 2\mu}{\lambda + \mu} \right] e^{-\frac{\omega z}{c}} e^{i(kx - \omega t)} \tag{29}$$

Tilt contribution for Sorrells’s [3] expression:

$$u_{\text{tilt}}^S = \frac{ig}{\omega^2} \frac{P_o}{2\mu} \left[\frac{\lambda + 2\mu}{\lambda + \mu} + \frac{\omega z}{c} \right] e^{-\frac{\omega z}{c}} e^{i(kx - \omega t)}. \tag{30}$$

We note that the effect of tilt, Equations (29) and (30), is the same at the surface of the medium ($z = 0$), as expected from the discussion above. However, Equation (29) for the complete solution does not contain the $\frac{\omega z}{c}$ dependent term, so the predicted tilt will decay more quickly with depth than the tilt predicted using Sorrells’s expression, (Equation (30)) or the actual displacements (Equations (27) and (28)). When $\frac{\omega z}{c}$ is large, i.e., has a large depth, the tilt correction for the horizontal displacement will be negligible. Furthermore, the horizontal and vertical displacements will be of equal magnitude. The required depth for this transition will be greater for the lower-frequency (longer-period) signals. Sorrells’s expression for the tilt contribution is proportional to w irrespective of depth in the medium, and will overpredict the tilt contribution as a function of depth.

The relative magnitude of the tilt correction with respect to u and w at the surface $z = 0$ are

$$\frac{u_{\text{tilt}}(0)}{u(0)} = \frac{g}{\omega c} \left[\frac{\alpha^2}{\beta^2} \right] \tag{31}$$

and

$$\frac{u_{\text{tilt}}(0)}{w(0)} = \frac{g}{\omega c}. \tag{32}$$

The importance of tilt is more pronounced in soft grounds. For $\omega < \frac{g}{c}$, which by assumption is of order one or less, the horizontal displacement associated with tilt at the surface will be larger than both the actual horizontal and vertical displacements. However, given the decay of the effect of tilt with depth discussed above, the sum of the actual and tilt contributions must be analyzed. For measurements below the ground surface, one cannot assume that if tilt dominates at the surface, it will dominate at all depths.

We also note that the sign change that occurs for horizontal displacement when

$$\frac{\omega z}{c} = \frac{\mu}{\lambda + \mu} \tag{33}$$

will occur at greater depth for the sum of horizontal displacement and tilt correction:

$$\frac{\omega z}{c} = \frac{g}{\omega c} \left[\frac{\lambda + 2\mu}{\lambda + \mu} \right] + \frac{\mu}{\lambda + \mu}. \tag{34}$$

The parameter $\frac{\omega z}{c}$ is an important factor in the behavior of the solutions. The relative decay of the tilt effect relative to the actual displacements is dependent on $\frac{\omega z}{c}$. When $\frac{\omega z}{c}$ is large, the tilt contribution is negligible, and horizontal displacement u and vertical displacement w are of equal magnitude. The change in sign of the horizontal displacement is also dependent on $\frac{\omega z}{c}$.

3. Results

In this section, representative examples are presented for the amplitude and decay with depth of the effective horizontal displacement and the vertical displacement. Equation (15a,b) are solved for φ_0 and ψ_0 using MATLAB [7], then Equations (12b), (13b) and (23) are used to evaluate the vertical displacements at the surface and at depths and the effective horizontal displacement at the surface and at depths. For comparison with Sorrells, the period $T = \frac{1}{f}$ is used as the independent variable in place of frequency.

These are exact results without any of the approximations used by Sorrells [3]. Figure 3 displays the surface values of the effective horizontal displacements (solid line) and the vertical displacements (dotted line) per μbar of pressure amplitude versus period for three cases from Sorrells [3]. Model 1 represents the case for unconsolidated soils with low values of α , β , and ρ , which explains the comparative maximum displacements among the three models. Values of α , β , and ρ for different geology are shown in Table 1.

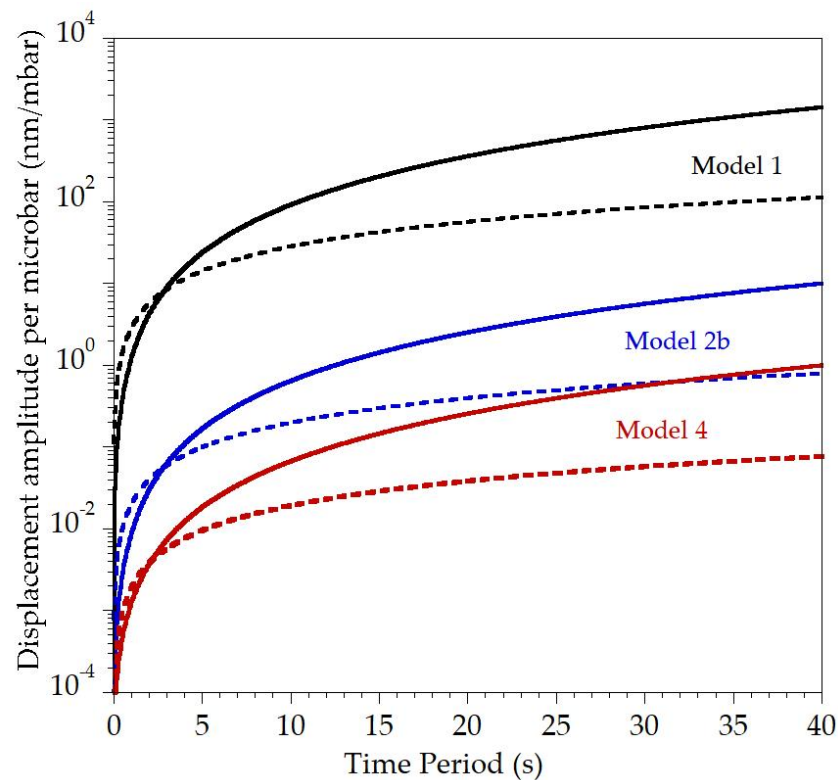


Figure 3. Exact calculation of total horizontal (solid line) and vertical (dotted line) displacement amplitude per microbar at the surface of an elastic half-space as a function of time period of a plane pressure wave moving at a speed of 5 m/s for Models 1, 2b, and 4.

Table 1. Model parameters used in the computation of total horizontal and vertical displacement at the surface caused by a plane pressure wave moving at a speed of 5 m/s.

Model No.	α (km/s)	β (km/s)	ρ (g/cm ³)	Geology
1	0.3	0.1	1.6	Unconsolidated sediments
2b	2.9	1.0	2.3	Sedimentary rock
4	5.8	3.25	2.85	Granites

Examination of Equations (27)–(30) shows that the principal factor effecting the magnitude of the displacement terms is the shear modulus $\mu = \rho\beta^2$, which varies by a factor of order 1000 between Model 1 and Model 4. For a given pressure amplitude, both effective horizontal displacement and vertical displacement increase with the increase in period but the vertical displacement is dominant for periods below 5 s. For periods greater than ~5 s, the effective horizontal displacement is greater than the vertical displacement. Figure 3 presents results explicitly for the surface of an elastic half-space and corresponds to results provided by Sorrell [3].

Figure 4 shows apparent ground motion caused by harmonic pressure fluctuations on the ground for different periods and depths. The total horizontal displacement ratio and vertical displacement ratio in Figure 4 are expressed as a function of depth (z);

$$\text{Horizontal displacement ratio (u)} = 20 \log_{10} \left[\frac{u_{\text{effective}}(z)}{w(0)} \right] \quad (35)$$

$$\text{Vertical displacement ratio (w)} = 20 \log_{10} \left[\frac{w(z)}{w(0)} \right]. \quad (36)$$

The results shown in Figure 4 are based on Model 4 and use the tilt expression corrected from Sorrells for horizontal displacement measured by a sensor deployed under the ground. Vertical displacements observed in Figure 4 across a wide range of periods of pressure variations associated with the atmosphere are comparable to Sorrells [3] and continually attenuate with an increase in depth, as suggested by Equation (28).

Sorrells's [3] expression for horizontal displacement (Equation (30)) shows that tilt attenuation is directly dependent on depth, and displays similar behavior to the attenuation of vertical displacement with depth. Since horizontal displacement has a tilt correction, from Equation (29) it can be seen that the size of tilt attenuates rapidly with increase in depth. This attenuation is different from Sorrells's s^3 expression because it does not contain the term $\frac{\omega z}{c}$ in the square brackets. Due to this, the total horizontal displacement exhibits different asymptotic behavior than the vertical displacement. The correct total displacement displays much larger attenuation at large depths.

From Figure 4a, it can be seen that at a short period (1.0 s) the size of tilt is small, and as a result the vertical displacement is larger than the effective horizontal displacement. For longer periods (Figure 4b–d), the effective horizontal displacement is larger. As depth increases, the effective horizontal displacement becomes smaller and eventually changes sign at a certain depth. The dips in the curve are where the sign changes occur. Beyond this depth, the horizontal and vertical displacements decay in a similar fashion. At very long periods (Figure 4e), it can be observed that the total horizontal displacement can be greater than the vertical displacement for a considerable depth (~275 m). Beyond 275 m, the vertical displacement is larger than the horizontal displacement.

Even if the model parameters are changed, the results do not change dramatically from the result presented in Figure 4 because the attenuation ratio does not contain the shear modulus and the ratio $\frac{\lambda+2\mu}{\lambda+\mu}$ does not vary greatly for a given elastic medium.

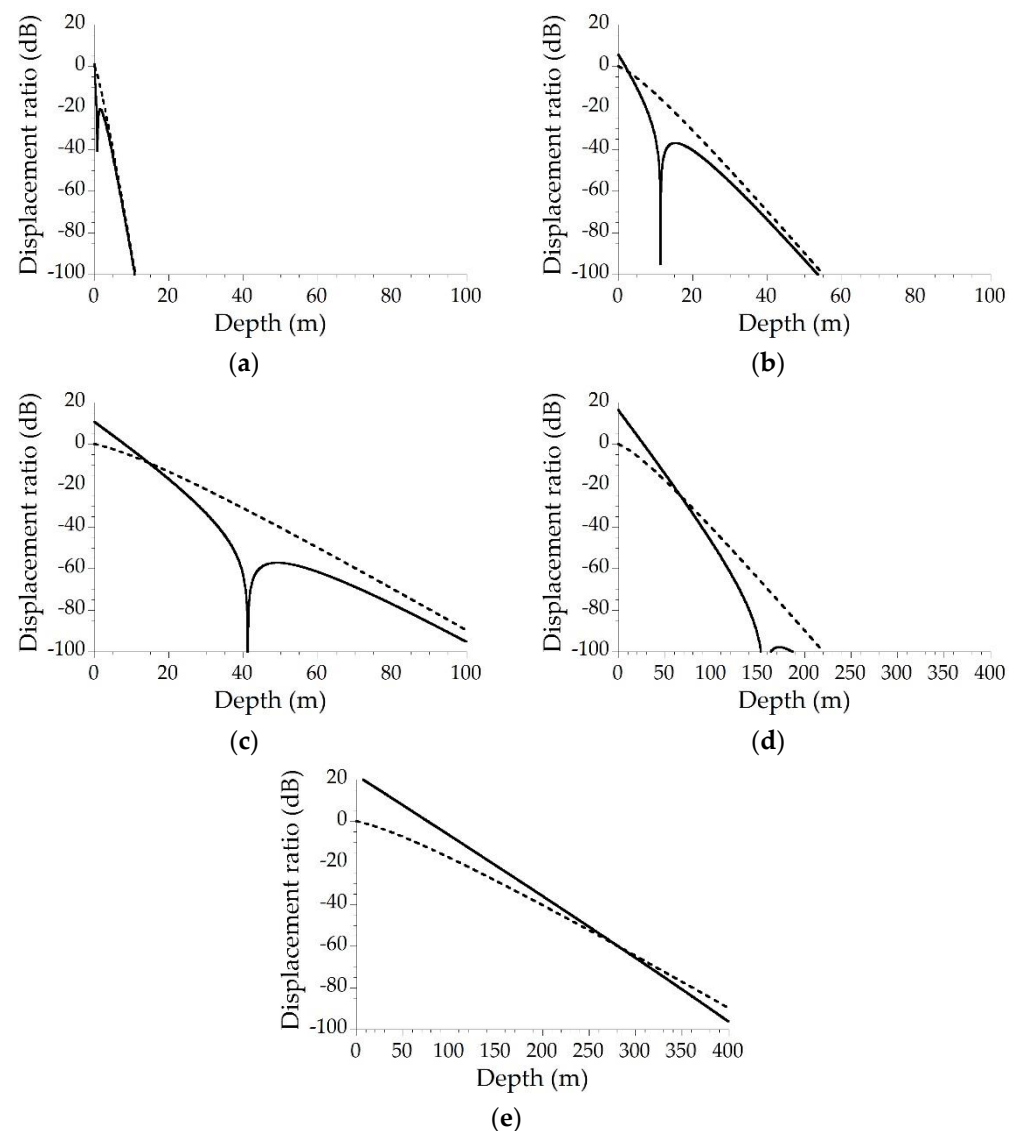


Figure 4. Ratio of total horizontal displacement (solid line) to vertical displacement at surface and vertical displacement (dotted line) to vertical displacement at surface at different depths for period of (a) 1 s, (b) 5 s, (c) 10 s, (d) 20 s, and (e) 40 s for model parameter with $\frac{\lambda+2\mu}{\lambda+\mu} = 1.5$.

4. Discussion

A thorough review of literature which cites Sorrells [3] using SCOPUS and Google Scholar was performed and the literature studied to see if the use of the incomplete expression for tilt had a significant impact on the published results.

The majority of the papers do not involve detailed calculations of the tilt contribution below the surface. These papers are divided into five classes which are analyzed in the following paragraphs:

Many papers just quote Sorrells [3] for the existence of horizontal and vertical displacements due to atmospheric pressure fluctuations on the earth's surface [8–49]. The correction has no effect on the results of these papers.

A second set of papers refers to Sorrells's [3] prediction of the exponential attenuation of the vertical and tilt contributions as a means of reducing noise on geophones, but do not perform any calculations with the equations [13,18,21,25,33,38,50–62]. Again, the details of the tilt decay with depth are inconsequential to the validity of these papers. Note that some of these papers are also included in the first set.

A third set of papers are concerned with seismic surface noise on other planets [63–78]. The constraints of planetary exploration limit the placement of the seismometers to the surface where Sorrells's [3] tilt calculation is correct; these are not affected by the correction discussed in this paper. An interesting extension of Sorrells's principles to dust devil detection is investigated in [57,63,69,75].

A smaller set of papers is those that reference Sorrells [3] but investigate phenomena outside the range of significance of the tilt correction. Included in this set are Ref. [1] and [2] which investigate seismic wind noise above 1 Hz. At the other extreme are papers [79–84] which investigate pressure effects on the ground displacement and tilt at very low frequencies ($f < 10^{-3}$ Hz) where the parameter $\omega z/c$ is negligible even for sensors employed at depths of hundreds of meters. In addition, the gravitational effect of the increased air mass above the sensor dominates the direct vertical displacement at these low frequencies.

Four papers adapt Sorrells's [3] calculations to sound coupling into the ground. The phase speed of the pressure fluctuations due to sound is on the order of the speed of sound at approximately 330 m/s or higher. For these cases the parameter $\omega z/c$ will be small, even for moderate frequencies and depths, so the horizontal tilt contribution is approximately the surface value. Weber [85] adapts Sorrells's [3] mathematical model to the problem of sonic boom coupling into the ground. Negaru [86] studied ambient infrasonic waves and corresponding seismic signals with borehole and surface sensors. Mauk [87] used seismic recordings to estimate volcanic explosivity from the infrasound levels inferred from the seismic measurements. De Angelis, McNutt, and Webley [88] studied ground coupling of atmospheric gravity waves into the ground using Sorrells's [3] results for vertical displacement, but did not study any horizontal components.

Sorrells's own papers subsequent to Ref. [3] do not correct the use of the single gradient instead of the curl for the tilt angle. Sorrells, McDonald, Der, and Herrin's "Earth motion caused by local atmospheric changes" [89] is an experimental study which only examines the vertical component of displacement and is unaffected by the correction of the tilt equation. Sorrells and Goforth's "Low-frequency earth motion generated by slowly propagating partially organized fields" [90] studies the transfer function between pressure fluctuations and surface displacements. The single-gradient expression given in Equation (21) of the paper is used to develop the measured horizontal displacement. This is correct for surface results, as explained in Section 2. Douze and Sorrells's "Prediction of pressure-generated earth motion using optimum filters" [91] is an experimental paper which examines the correlation between surface pressure fluctuation and surface displacements. Our literature search has not found any correction or extension of the original paper in Sorrells's subsequent publications.

Dybing, Ringler, Wilson, and Anthony's "Characteristics and spatial variability of wind noise on near-surface broadband seismometers" [92] investigates correlations between measured wind speed and seismic measurements. We note that the correlations are much shorter than those reported in other papers, but also that the measurement site has many buildings and trees to affect the fetch of the wind, and therefore its correlation properties. Table 2 of this reference displays linear fits to RMS velocity curves versus RMS wind speed measurements. For sensors near the surface, the horizontal components are much larger than the corresponding vertical components which display the results of tilt on the measurements. In contrast, the results reported at 145 m show components of the horizontal and vertical of the same order of magnitude. This may indicate that the attenuation predicted using the full expression for tilt is more realistic than the tilt correction using the single gradient.

De Angelis and Bodin in "Watching the wind: Seismic data contamination at long periods due to atmospheric pressure-field-induced tilting" [93] study the effect of wind-induced tilt on near-surface horizontal data. Their Figure 9 displays the attenuation versus depth of tilt contribution using Sorrells's [3] results. The results, using the complete expression, display a zero and a sign change in the total horizontal effective velocity, and much enhanced attenuation in the range displayed.

Wolin, van der Lee, Bollman, Weins, Revenaugh, Darbyshire, Frederiksen, Stein, and Wysession in "Seasonal and diurnal variations in long-period noise at SPREE stations: The

influence of soil characteristics on shallow stations' performance" [94] analyze seismic noise using Sorrells's [3] results, but all measurements are near-surface and are therefore not affected by the correct tilt calculation.

Tanimoto and Wang in "*Low-frequency seismic noise characteristics from the analysis of collocated seismic and pressure data*" [95] use pressure and vertical and horizontal seismic velocity data from stations in the USArray Transportable Array to estimate the rigidity of the surface in the first few hundred meters of depth. Sorrells's [3] formulae are used in these calculations. The predicted depth dependence of the vertical velocity is used to argue that the measurement is only sensitive to rigidities nearer to the surface. The implication of the increased attenuation of the tilt contribution discussed in Section 2 is that the horizontal velocity should be determined by the properties closer to the surface than the vertical velocities.

The most intriguing paper referencing Sorrells [3] is Tanimoto and Wang's "*Theory for deriving shallow elasticity structure from collocated seismic and pressure data*" [4]. This paper uses Sorrells's assumptions to develop an inversion scheme for estimating ground properties as a function of depth from measurements of the vertical and horizontal seismic velocities, as well as pressure fluctuations at the ground surface. In this paper they specify the correct expression for the tilt angle in the ground (their Equation (25)), but note that the single derivative (their Equation (27)) is correct near the ground surface, and use this expression throughout the paper. We have not repeated their calculations, but we note that determining the extent of the influence of the ground properties from the predicted decay with depth is important to the inversion. Our results show that the tilt decays more quickly with depth and should be more sensitive to near-surface properties than vertical displacement.

Tanimoto and Wang [4] estimate the wind speed c from the ratio of the horizontal to vertical velocities and find that the best fit is obtained with a wind speed that increases with frequency. Priestley [96] and Shields [97] measured the correlation properties of the wind pressure at infrasonic frequencies and found that the convection velocity increased with decreasing frequency, concluding that the larger scales were sampling higher in the atmospheric boundary layer where the wind speed is greater. This may be an indication that the theory of Ref. [4] needs to be modified to use the correct expression for tilt under the surface.

5. Conclusions

The use of the complete expression for the tilt angle in the ground has a large effect on the predicted horizontal displacements below the surface. The effect is important when $\omega z/c$ is moderately large and $g/(\omega c) > 1$. For depths of a few hundred meters, this limits the significance of the correction to frequencies between 0.1 Hz and 0.01 Hz.

Since most of the literature which cites Sorrells [3] is concerned with surface measurements or is restricted to vertical displacements, the correction of the tilt angle has little or no effect. We have identified one borehole measurement [91] which may reflect the enhanced attenuation of the tilt contribution, and a few theoretical plots which should be modified. We speculate that the additional attenuation of the tilt correction may affect the inversions of Ref. [4].

The prediction of large contributions of horizontal noise may have discouraged measurements of the horizontal displacement at depths. Many papers limit measurements to the vertical displacements based on the prediction of Sorrells [3] that the horizontal will suffer much larger noise contributions from the wind.

Finally, the predicted complex nature of the total horizontal displacement offers the possibility of sensitive determination of ground properties through combined horizontal and vertical measurements at different burial depths in the ground. At an appropriate fixed depth, the sign reversal displayed in Figure 4 will also occur in plots of horizontal displacement versus frequency, so that Equation (34) can also be used to evaluate ground properties.

Author Contributions: R.R. developed the theoretical formalism, performed the analytic calculations, and provided the original draft. Both R.R. and B.K. performed the numerical simulations. R.R., B.K., and C.J.H. contributed to the interpretation and writing—review and editing. C.J.H. was responsible

for project administration and funding acquisition. All authors have read and agreed to the published version of the manuscript.

Funding: Bipin Koirala was supported by the BASS summer research program at the University of Mississippi, National Center for Physical Acoustics. This work was supported in part by the U.S. Department of Agriculture under Non-Assistance Cooperative Agreement 58-6060-6-009 and the Office of Naval Research under Award No. N00014-18-1-2489. Any opinions, findings, conclusions, or recommendations expressed in this publication are those of the author(s) and do not necessarily reflect the view of the respective Federal agencies.

Acknowledgments: We would like to acknowledge the assistance in researching the literature base of Jason Burton, former Lead STEM Librarian at the University of Mississippi.

Conflicts of Interest: The authors declare no conflict of interest.

References

- Naderyan, V.; Hickey, C.J.; Rasper, R. Wind-induced ground motion. *J. Geophys. Res. Solid Earth* **2016**, *121*, 917–930. [\[CrossRef\]](#)
- Mohammadi, M.; Hickey, C.J.; Rasper, R.; Naderyan, V. Wind-induced ground motion: Dynamic model and nonuniform structure for ground. *J. Geophys. Res. Solid Earth* **2019**, *124*, 8478–8490. [\[CrossRef\]](#)
- Sorrells, G.G. A preliminary investigation into the relationship between long-period seismic noise and local fluctuations in the atmospheric pressure field. *Geophys. J. R. Astr. Soc.* **1971**, *26*, 71–82. [\[CrossRef\]](#)
- Tanimoto, T.; Wang, J. Theory for deriving shallow elasticity structure from collocated seismic and pressure data. *J. Geophys. Res. Solid Earth* **2019**, *124*, 5811–5835. [\[CrossRef\]](#)
- Brekhovskikh, L.M. Plane Waves in Discretely Layered Media. In *Waves in Layered Media*, 2nd ed.; Frankiel, F.N., Temple, G., Eds.; Beyer, R.T., Translator; Academic Press: San Diego, CA, USA, 1980; pp. 1–129.
- Fetter, A.L.; Walecka, J.D. Elastic Continua. In *Theoretical Mechanics of Particles and Continua*; Zappa, C.R., Eichberg, M., Eds.; McGraw-Hill: New York, NY, USA, 1980; pp. 459–479.
- Release, S.T. *MATLAB*; The MathWorks: Natick, MA, USA, 2018.
- Altmann, J. Acoustic-seismic detection of ballistic-missile launches for cooperative early warning of nuclear attack. *Sci. Glob. Secur.* **2005**, *13*, 129–168. [\[CrossRef\]](#)
- Ansari, A.; Hosseini, K.A. Broadband seismic network of Iran and increasing quality of seismic recordings. *Seismol. Res. Lett.* **2014**, *85*, 878–888. [\[CrossRef\]](#)
- Anthony, R.E.; Aster, R.C.; Ryan, S.; Rathburn, S.; Baker, M.G. Measuring mountain river discharge using seismographs emplaced within the hyporheic zone. *J. Geophys. Res. Earth Surf.* **2018**, *123*, 210–228. [\[CrossRef\]](#)
- Anthony, R.E.; Aster, R.C.; Weins, D.; Nyblade, A.; Anandakrishnan, S.; Huerta, A.; Winberry, J.P.; Wilson, T.; Rowe, C. The seismic noise environment of Antarctica. *Seismol. Res. Lett.* **2014**, *86*, 89–100. [\[CrossRef\]](#)
- Barruol, G.; Reymond, D.; Fontaine, F.R.; Hyvernaud, O.; Maurer, V.; Maamaatuaiahutapu, K. Characterizing swells in the southern Pacific from seismic and infrasonic noise analyses. *Geophys. J. Int.* **2006**, *164*, 516–542. [\[CrossRef\]](#)
- Beauduin, R.; Lognonné, P.; Montagner, J.P.; Cacho, S.; Karczewski, J.F.; Morand, M. The effects of the atmospheric pressure changes on seismic signals or how to improve the quality of a station. *Bull. Seismol. Soc. Am.* **1996**, *86*, 1760–1769. [\[CrossRef\]](#)
- Block, B.; Dratler, J., Jr. Improvements in the wide-band vertical quartz torsion accelerometer. *J. Geophys. Res.* **1972**, *77*, 3678–3689. [\[CrossRef\]](#)
- Bodin, P.; Smith, K.; Horton, S.; Hwang, H. Microtremor observations of deep sediment resonance in metropolitan Memphis, Tennessee. *Eng. Geol.* **2001**, *62*, 159–168. [\[CrossRef\]](#)
- Díaz, J. On the origin of the signals observed across the seismic spectrum. *Earth-Sci. Rev.* **2016**, *161*, 224–232. [\[CrossRef\]](#)
- Díaz, J.; Villaseñor, A.; Morales, J.; Pazos, A.; Córdoba, D.; Pulgar, J.; García-Lobón, J.L.; Harnafi, M.; Carbonell, R.; Gallart, J. Background noise characteristics at the IberArray broadband seismic network. *Bull. Seismol. Soc. Am.* **2010**, *100*, 618–628. [\[CrossRef\]](#)
- Dratler, J.; Block, B. A wide band horizontal accelerometer with preliminary Earth normal mode and seismic investigations. *Geophys. J. Int.* **1972**, *27*, 337–367. [\[CrossRef\]](#)
- Duputel, Z.; Rivera, L.; Fukahata, Y.; Kanamori, H. Uncertainty estimations for seismic source inversions. *Geophys. J. Int.* **2012**, *190*, 1243–1256. [\[CrossRef\]](#)
- Gebauer, A.; Kroner, C.; Jahr, T. The influence of topographic and lithologic features on horizontal deformations. *Geophys. J. Int.* **2009**, *177*, 586–602. [\[CrossRef\]](#)
- Gebauer, A.; Steffen, H.; Kroner, C.; Jahr, T. Finite element modelling of atmosphere loading effects on strain, tilt and displacement at multi-sensor stations. *Geophys. J. Int.* **2010**, *181*, 1593–1612. [\[CrossRef\]](#)
- Goodman, D.; Yamamoto, T.; Trevorrow, M.; Abbott, C.; Turgut, A.; Badiy, M.; Ando, K. Directional spectra observations of seafloor microseisms from an ocean-bottom seismometer array. *J. Acoust. Soc. Am.* **1989**, *86*, 2309–2317. [\[CrossRef\]](#)

23. Green, D.N.; Le Pichon, A.; Ceranna, L.; Evers, L. Ground Truth Events: Assessing the Capability of Infrasound Networks Using High Resolution Data Analyses. In *Infrasound Monitoring for Atmospheric Studies*; Le Pichon, A., Blanc, E., Hauchorne, A., Eds.; Springer: Dordrecht, Switzerland, 2010; pp. 599–625.
24. Hu, W.; Pryor, S.C.; Letson, F.; Tytell, J.; Barthelmie, R.J. Investigation of gust-seismic relationships and applications to gust detection. *J. Geophys. Res. Atmos.* **2017**, *122*, 140–151. [[CrossRef](#)]
25. Hutt, C.R.; Ringler, A.T.; Gee, L.S. Broadband seismic noise attenuation versus depth at the Albuquerque seismological laboratory. *Bull. Seismol. Soc. Am.* **2017**, *107*, 1402–1412. [[CrossRef](#)]
26. Johnson, C.W.; Meng, H.; Vernon, F.; Ben-Zion, Y. Characteristics of ground motion generated by wind interaction with trees, structures, and other surface obstacles. *J. Geophys. Res. Solid Earth* **2019**, *124*, 8519–8539. [[CrossRef](#)]
27. Kroner, C.; Jahr, T.; Kuhlmann, S.; Fischer, K.D. Pressure-induced noise on horizontal seismometer and strainmeter records evaluated by finite element modelling. *Geophys. J. Int.* **2005**, *161*, 167–178. [[CrossRef](#)]
28. Li, G.; Li, Y.; Yang, B. Seismic exploration random noise on land: Modeling and application to noise suppression. *IEEE Trans. Geosci. Remote Sens.* **2017**, *55*, 4668–4681. [[CrossRef](#)]
29. Mauk, F.J.; Mahrer, K.D. Use of long-period seismometers to determine induced fracture geometry. *SPE Prod. Eng.* **1988**, *3*, 192–200. [[CrossRef](#)]
30. Mucciarelli, M.; Gallipoli, M.R.; Di Giacomo, D.; Di Nota, F.; Nino, E. The influence of wind on measurements of seismic noise. *Geophys. J. Int.* **2005**, *161*, 303–308. [[CrossRef](#)]
31. Panou, A.A.; Theodulidis, N.P.; Hatzidimitriou, P.M.; Savvaidis, A.S.; Papazachos, C.B. Reliability of ambient noise horizontal-to-vertical spectral ratio in urban environments: The case of Thessaloniki City (Northern Greece). *Pure Appl. Geophys.* **2005**, *162*, 891–912. [[CrossRef](#)]
32. Ringler, A.T.; Wilson, D.C.; Zürn, W.; Anthony, R.E. Rayleigh wave ellipticity measurement uncertainty across the IRIS/USGS and New China Digital Seismograph Networks. *Geophys. J. Int.* **2018**, *217*, 219–237. [[CrossRef](#)]
33. Rohde, M.D.; Ringler, A.T.; Hutt, C.R.; Wilson, D.C.; Holland, A.A.; Sandoval, L.D.; Storm, T. Characterizing local variability in long-period horizontal tilt noise. *Seismol. Res. Lett.* **2017**, *88*, 822–830. [[CrossRef](#)]
34. Rouland, D.; Condis, C.; Roullet, G. Overlooked earthquakes on and around the Antarctica plate: Identification and location of 1999 shallow depth events. *Tectonophysics* **2003**, *376*, 1–17. [[CrossRef](#)]
35. Roullet, G.; Crawford, W. Analysis of ‘background’ free oscillations and how to improve resolution by subtracting the atmospheric pressure signal. *Phys. Earth Planet. Inter.* **2000**, *121*, 325–338. [[CrossRef](#)]
36. Steffen, H.; Kuhlmann, S.; Jahr, T.; Kroner, C. Numerical modelling of the barometric pressure-induced noise in horizontal components for the observatories Moxa and Schiltach. *J. Geodyn.* **2006**, *41*, 242–252. [[CrossRef](#)]
37. Steim, J.M. Theory and Observations-Instrumentation for Global and Regional Seismology. In *Treatise on Geophysics: Volume 1 Deep Earth Seismology*; Romanowicz, B., Dziewonski, A., Eds.; Elsevier Science: San Diego, CA, USA, 2015; pp. 29–74.
38. Stutzmann, E.; Roullet, G.; Astiz, L. GEOSCOPE station noise levels. *Bull. Seismol. Soc. Am.* **2000**, *90*, 690–701. [[CrossRef](#)]
39. Suda, N.; Nawa, K.; Fukao, Y. Earth’s background free oscillations. *Science* **1998**, *279*, 2089–2091. [[CrossRef](#)]
40. Tanimoto, T. Interaction of solid Earth, atmosphere, and ionosphere. *Treatise Geophysics.* **2007**, *4*, 421–444.
41. Tanimoto, T.; Valovcin, A. Existence of the threshold pressure for seismic excitation by atmospheric disturbances. *Geophys. Res. Lett.* **2016**, *43*, 11–202. [[CrossRef](#)]
42. Tape, C.; Christensen, D.; Moore-Driskell, M.M.; Sweet, J.; Smith, K. Southern Alaska Lithosphere and Mantle Observation Network (SALMON): A seismic experiment covering the active arc by road, boat, plane, and helicopter. *Seismol. Res. Lett.* **2017**, *88*, 1185–1202. [[CrossRef](#)]
43. Valovcin, A.; Tanimoto, T. Modeling the excitation of seismic waves by the Joplin tornado. *Geophys. Res. Lett.* **2017**, *44*, 10–256. [[CrossRef](#)]
44. Vila, J.; Macià, R. The broadband seismic station CADI (Tunel del Cadi, Eastern Pyrenees), part II: Long-period variations of background noise. *Bull. Seismol. Soc. Am.* **2002**, *92*, 3329–3334. [[CrossRef](#)]
45. Webb, S.C. Broadband seismology and noise under the ocean. *Rev. Geophys.* **1998**, *36*, 105–142. [[CrossRef](#)]
46. Widmer, R.; Zürn, W.; Masters, G. Observation of low-order toroidal modes from the 1989 Macquarie Rise event. *Geophys. J. Int.* **1992**, *111*, 226–236. [[CrossRef](#)]
47. Xia, Y.; Ni, S.; Tape, C. Multipathing Rayleigh waves from long-distance noise cross correlation along an ocean-continent boundary (Alaska to California). *Geophys. Res. Lett.* **2018**, *45*, 6051–6060. [[CrossRef](#)]
48. Yang, C.F.; Chi, W.C.; Lai, Y.J. Seismically detected ground tilts Induced by precipitation and fluvial processes: An example from Taiwan. *J. Geophys. Res. Solid Earth* **2018**, *123*, 4814–4828. [[CrossRef](#)]
49. Yang, Z.; Sheehan, A.F.; Collins, J.A.; Laske, G. The character of seafloor ambient noise recorded offshore New Zealand: Results from the MOANA ocean bottom seismic experiment. *Geochem. Geophys. Geosyst.* **2012**, *13*, 10011. [[CrossRef](#)]
50. Adair, R.G.; Orcutt, J.A.; Jordan, T.H. Low-frequency noise observations in the deep ocean. *J. Acoust. Soc. Am.* **1986**, *80*, 633–645. [[CrossRef](#)]
51. Custódio, S.; Dias, N.A.; Caldeira, B.; Carrilho, F.; Carvalho, S.; Díaz, J.; Narciso, J.; Madureira, G.; Matias, L.; Haberland, C.; et al. Ambient noise recorded by a dense broadband seismic deployment in western Iberia. *Bull. Seismol. Soc. Am.* **2014**, *104*, 2985–3007. [[CrossRef](#)]

52. Doody, C.D.; Ringler, A.T.; Anthony, R.E.; Wilson, D.C.; Holland, A.A.; Hutt, C.R.; Sandoval, L.D. Effects of thermal variability on broadband seismometers: Controlled experiments, observations, and implications. *Bull. Seismol. Soc. Am.* **2018**, *108*, 493–502. [[CrossRef](#)]
53. Hayman, M.B. Downhole Seismometers. In *Encyclopedia of Earthquake Engineering*; Beers, M., Kougoumtzoglou, I.A., Patelli, E., Au, S.-K., Eds.; Springer: Berlin/Heidelberg, Germany, 2014; pp. 1–22. [[CrossRef](#)]
54. Li, Y.; Prothero, W., Jr.; Thurber, C.; Butler, R. Observations of ambient noise and signal coherency on the island of Hawaii for teleseismic studies. *Bull. Seismol. Soc. Am.* **1994**, *84*, 1229–1242. [[CrossRef](#)]
55. Melton, B.S. The sensitivity and dynamic range of inertial seismographs. *Rev. Geophys.* **1976**, *14*, 93–116. [[CrossRef](#)]
56. Montagner, J.-P.; Karczewski, J.-F.; Romanowicz, B.; Bouaricha, S.; Lognonne, P.; Roult, G.; Stutzmann, E.; Thiriot, J.-L.; Brion, J.; Dole, B.; et al. The French Pilot Experiment OFM-SISMOBS: First scientific results on noise level and event detection. *Phys. Earth Planet. Inter.* **1994**, *84*, 321–336. [[CrossRef](#)]
57. Peterson, J.; Butler, H.M.; Holcomb, L.G.; Hutt, C.R. The seismic research observatory. *Bull. Seismol. Soc. Am.* **1976**, *66*, 2049–2068. [[CrossRef](#)]
58. Peterson, J.; Orsini, N.A. Seismic research observatories: Upgrading the worldwide seismic data network. *Eos Trans. Am. Geophys. Union* **1976**, *57*, 548–556. [[CrossRef](#)]
59. Ringler, A.T.; Hagerty, M.T.; Holland, J.; Gonzales, A.; Gee, L.S.; Edwards, J.D. The data quality analyzer: A quality control program for seismic data. *Comput. Geosci.* **2015**, *76*, 96–111. [[CrossRef](#)]
60. Ringler, A.T.; Steim, J.M.; van Zandt, T.; Hutt, C.R.; Wilson, D.C.; Storm, T.L. Potential improvements in horizontal very broadband seismic data in the IRIS/USGS component of the Global Seismic Network. *Seismol. Res. Lett.* **2015**, *87*, 81–89. [[CrossRef](#)]
61. Ringler, A.T.; Wilson, D.C.; Storm, T.; Marshall, B.; Hutt, C.R.; Holland, A.A. Noise reduction in long-period seismograms by way of array summing. *Bull. Seismol. Soc. Am.* **2016**, *106*, 1991–1997. [[CrossRef](#)]
62. Webb, S.C.; Lee, W.H.K. Seismic noise on land and on the seafloor. *Int. Handb. Earthq. Eng. Seismol.* **2002**, *81*, 305–318.
63. Kenda, B.; Lognonné, P.; Spiga, A.; Kawamura, T.; Kedar, S.; Banerdt, W.B.; Lorenz, R.; Banfield, D.; Golembek, M. Modeling of ground deformation and shallow surface waves generated by Martian dust devils and perspectives for near-surface structure inversion. *Space Sci. Rev.* **2017**, *211*, 501–524. [[CrossRef](#)]
64. Lognonné, P.; Zharkov, V.N.; Karczewski, J.F.; Romanowicz, B.; Menvielle, M.; Poupinet, G.; Brient, B.; Cavoit, C.; Desautez, A.; Dole, R.; et al. The seismic OPTIMISM experiment. *Planet. Space Sci.* **1998**, *46*, 739–747. [[CrossRef](#)]
65. Lognonné, P.; Beyneix, J.G.; Banerdt, W.B.; Cacho, S.; Karczewski, J.F.; Morand, M. Ultra broad band seismology on InterMarsNet. *Planet. Space Sci.* **1996**, *44*, 1237–1249. [[CrossRef](#)]
66. Lognonné, P.; Johnson, C. Planetary Seismology. In *Treatise on Geophysics*; Elsevier: Amsterdam, The Netherlands, 2007; Volume 10, pp. 69–122.
67. Lognonné, P.; Mosser, B. Planetary seismology. *Surv. Geophys.* **1993**, *14*, 239–302. [[CrossRef](#)]
68. Lorenz, R.D. Planetary seismology—Expectations for lander and wind noise with application to Venus. *Planet. Space Sci.* **2012**, *62*, 86–96. [[CrossRef](#)]
69. Lorenz, R.D.; Kedar, S.; Murdoch, N.; Lognonné, P.; Kawamura, T.; Mimoun, D.; Bruce Banerdt, W. Seismometer detection of dust devil vortices by ground tilt. *Bull. Seismol. Soc. Am.* **2015**, *105*, 3015–3023. [[CrossRef](#)]
70. Mège, D.; Gurgurewicz, J.; Grygorczuk, J.; Wiśniewski, Ł.; Thornell, G. The Highland Terrain Hopper (HOPTER): Concept and use cases of a new locomotion system for the exploration of low gravity Solar System bodies. *Acta Astronaut.* **2016**, *121*, 200–220. [[CrossRef](#)]
71. Mimoun, D.; Murdoch, N.; Lognonné, P.; Hurst, K.; Pike, W.T.; Hurley, J.; Nébut, T.; Banerdt, W.B.; SEIS Team. The noise model of the SEIS seismometer of the InSight mission to Mars. *Space Sci. Rev.* **2017**, *211*, 383–428. [[CrossRef](#)]
72. Murdoch, N.; Kenda, B.; Kawamura, T.; Spiga, A.; Lognonné, P.; Mimoun, D.; Banerdt, W.B. Estimations of the seismic pressure noise on Mars determined from Large Eddy Simulations and demonstration of pressure decorrelation techniques for the InSight mission. *Space Sci. Rev.* **2017**, *211*, 457–483. [[CrossRef](#)]
73. Murdoch, N.; Mimoun, D.; Garcia, R.F.; Rapin, W.; Kawamura, T.; Lognonné, P.; Banfield, D.; Banerdt, W.B. Evaluating the wind-induced mechanical noise on the InSight seismometers. *Space Sci. Rev.* **2017**, *211*, 429–455. [[CrossRef](#)]
74. Murdoch, N.; Mimoun, D.; Lognonné, P.; Garcia, R.; Kawamura, T. Environmental noise contributors on the InSight seismometers. *Eur. Planet. Sci. Congr.* **2018**, *8*, 2.
75. Murphy, J.; Steakley, K.; Balme, M.; Deprez, G.; Esposito, F.; Kahanpää, H.; Lemmon, M.; Lorenz, R.; Murdoch, N.; Neakrase, L.; et al. Field measurements of terrestrial and Martian dust devils. *Space Sci. Rev.* **2016**, *203*, 39–87. [[CrossRef](#)]
76. Pou, L.; Mimoun, D.; Lognonné, P.; Garcia, R.F.; Karatekin, O.; Nonon-Latapie, M.; Llorca-Cejudo, R. High precision SEIS calibration for the InSight mission and its applications. *Space Sci. Rev.* **2019**, *215*, 6. [[CrossRef](#)]
77. Reiss, D.; Lorenz, R.D. Dust devil track survey at Elysium Planitia, Mars: Implications for the InSight landing sites. *Icarus* **2016**, *266*, 315–330. [[CrossRef](#)]
78. Spiga, A.; Banfield, D.; Teanby, N.A.; Forget, F.; Lucas, A.; Kenda, B.; Manfredi, J.A.R.; Widmer-Schnidrig, R.; Murdoch, N.; Lemmon, M.T.; et al. Atmospheric science with InSight. *Space Sci. Rev.* **2018**, *214*, 109. [[CrossRef](#)]
79. Sobolev, G.A.; Zakrzhevskaya, N.A.; Migunov, I.N.; Sobolev, D.G. Migration of pulsations after earthquakes. *Izv. Phys. Solid Earth* **2017**, *53*, 493–517. [[CrossRef](#)]

80. Shved, G.M.; Ermolenko, S.I.; Karpova, N.V.; Wendt, S.; Jacobi, C. Detecting global atmospheric oscillations by seismic instruments. *Izv. Phys. Solid Earth* **2013**, *49*, 278–288. [[CrossRef](#)]
81. Shved, G.M.; Karpova, N.V.; Petrova, L.N.; Orlov, E.G.; Ermolenko, S.I. Steady-frequency waves at intradiurnal periods from simultaneous co-located microbarometer and seismometer measurements: A case study. *Ann. Geophys.* **2011**, *29*, 1153–1167. [[CrossRef](#)]
82. Zürn, W.; Exß, J.; Steffen, H.; Kroner, C.; Jahr, T.; Westerhaus, M. On reduction of long-period horizontal seismic noise using local barometric pressure. *Geophys. J. Int.* **2007**, *171*, 780–796. [[CrossRef](#)]
83. Zürn, W.; Meurers, B. Clear evidence for the sign-reversal of the pressure admittance to gravity near 3 mHz. *J. Geodyn.* **2009**, *48*, 371–377. [[CrossRef](#)]
84. Zürn, W.; Wielandt, E. On the minimum of vertical seismic noise near 3 mHz. *Geophys. J. Int.* **2007**, *168*, 647–658. [[CrossRef](#)]
85. Weber, G. Sonic boom exposure effects II. 1: Structures and terrain. *J. Sound Vib.* **1972**, *20*, 505–509. [[CrossRef](#)]
86. Negraru, P.T. Application of seismo-acoustic signals to the study of local site effects. *Acta Geophys.* **2010**, *58*, 1021–1039. [[CrossRef](#)]
87. Mauk, F.J. Utilization of seismically recorded infrasonic-acoustic signals to monitor volcanic explosions: The El Chichon Sequence 1982—A case study. *J. Geophys. Res. Solid Earth* **1983**, *88*, 10385–10401. [[CrossRef](#)]
88. De Angelis, S.; McNutt, S.R.; Webley, P.W. Evidence of atmospheric gravity waves during the 2008 eruption of Okmok volcano from seismic and remote sensing observations. *Geophys. Res. Lett.* **2011**, *38*, L10303. [[CrossRef](#)]
89. Sorrells, G.G.; McDonald, J.A.; Der, Z.A.; Herrin, E. Earth motion caused by local atmospheric pressure changes. *Geophys. J. Int.* **1971**, *26*, 83–98. [[CrossRef](#)]
90. Sorrells, G.G.; Goforth, T.T. Low-frequency earth motion generated by slowly propagating partially organized pressure fields. *Bull. Seismol. Soc. Am.* **1973**, *63*, 1583–1601. [[CrossRef](#)]
91. Douze, E.J.; Sorrells, G.G. Prediction of pressure-generated earth motion using optimum filters. *Bull. Seismol. Soc. Am.* **1975**, *65*, 637–650. [[CrossRef](#)]
92. Dybing, S.N.; Ringler, A.T.; Wilson, D.C.; Anthony, R.E. Characteristics and spatial variability of wind noise on near-surface broadband seismometers. *Bull. Seismol. Soc. Am.* **2019**, *109*, 1082–1098. [[CrossRef](#)]
93. De Angelis, S.; Bodin, P. Watching the wind: Seismic data contamination at long periods due to atmospheric pressure-field-induced tilting. *Bull. Seismol. Soc. Am.* **2012**, *102*, 1255–1265. [[CrossRef](#)]
94. Wolin, E.; van der Lee, S.; Bollmann, T.A.; Wiens, D.A.; Revenaugh, J.; Darbyshire, F.A.; Fredrickson, A.W.; Stein, S.; Wyssession, M.E. Seasonal and diurnal variations in long-period noise at SPREE stations: The influence of soil characteristics on shallow stations' performance. *Bull. Seismol. Soc. Am.* **2015**, *105*, 2433–2452. [[CrossRef](#)]
95. Tanimoto, T.; Wang, J. Low-frequency seismic noise characteristics from the analysis of co-located seismic and pressure data. *J. Geophys. Res. Solid Earth* **2018**, *123*, 5853–5885. [[CrossRef](#)]
96. Priestly, J.T. *Correlation Studies of Pressure Fluctuations on the Ground Beneath a Turbulent Boundary Layer*; National Bureau of Standards Report No. 8942; University of Maryland: Gaithersburg, MA, USA, 1965.
97. Shields, F.D. Low-frequency wind noise correlation in microphone arrays. *J. Acoust. Soc. Am.* **2005**, *117*, 3489–3496. [[CrossRef](#)]